Multiband Superconductivity in the Chevrel Phases $SnMo_6S_8$ and $PbMo_6S_8$

A. P. Petrović,[1] R. Lortz,[2] G. Santi,[1] C. Berthod,[1] C. Dubois,[1] M. Decroux,[1] A. Demuer,[3] A. B. Antunes,[3] A. Paré,[3] D. Salloum,[4] P. Gougeon,[4] M. Potel,[4] and Ø. Fischer[1]

[1]*DPMC-MaNEP, Université de Genève, Quai Ernest-Ansermet 24, 1211 Genève 4, Switzerland*
[2]*Department of Physics, The Hong Kong University of Science and Technology, Clear Water Bay, Kowloon, Hong Kong*
[3]*Laboratoire des Champs Magnétiques Intenses CNRS, 25 rue des Martyrs, B.P. 166, 38042 Grenoble Cedex 9, France*
[4]*Sciences Chimiques, CSM UMR CNRS 6226, Université de Rennes 1, Avenue du Général Leclerc, 35042 Rennes Cedex, France*

(Received 29 June 2010; published 6 January 2011)

Sub-Kelvin scanning tunneling spectroscopy in the Chevrel phases $SnMo_6S_8$ and $PbMo_6S_8$ reveals two distinct superconducting gaps with $\Delta_1 = 3$ meV, $\Delta_2 \sim 1.0$ meV and $\Delta_1 = 3.1$ meV, $\Delta_2 \sim 1.4$ meV, respectively. The gap distribution is strongly anisotropic, with Δ_2 predominantly seen when scanning across unit-cell steps on the (001) sample surface. The spectra are well fitted by an anisotropic two-band BCS *s*-wave gap function. Our spectroscopic data are confirmed by electronic heat capacity measurements, which also provide evidence for a twin-gap scenario.

DOI: 10.1103/PhysRevLett.106.017003 PACS numbers: 74.70.Dd, 74.20.Rp, 74.25.Bt, 74.55.+v

Among the vast zoo of poorly understood superconductors, Chevrel phases (CPs) stand out for their high upper critical fields H_{c2}, many of which exceed the Pauli limit [1]. These materials were first synthesized in 1971 [2] and enjoyed a wealth of attention in the early 1980s. Unfortunately, the discovery of the cuprate superconductors largely swept CPs under the laboratory carpet, despite a lack of detailed understanding of their large H_{c2} values. A multiband scenario (incorporating strong-coupling effects and enhanced spin-orbit scattering) was suggested as a possible explanation [3], but until now this hypothesis has remained experimentally unexplored.

Multiband superconductivity was first proposed 50 years ago as a potential avenue for increasing critical temperatures [4]. Each band at the Fermi level E_F may exhibit a superconducting gap with distinct magnitude and momentum dependence, while interband scattering can increase both H_{c2} and the transition temperature T_c. However, with the exception of some transition metal calorimetric data [5] and tunneling in doped $SrTiO_3$ [6], multiband superconductivity remained a largely theoretical concept until the discovery of MgB_2 in 2001 revived interest in the field [7]. In this material, superconductivity in the quasi-2D σ band induces coherence in the quasi-3D π band with an unexpectedly high T_c of 39 K. The two gaps have been imaged by a variety of techniques, including local spectroscopic [8] and bulk thermodynamic approaches [9]. Recently, multiband features have been found in borocarbides [10], sesquicarbides [11], skutterudites [12], and pnictides [13]. CPs and pnictides share similar anomalously large values of H_{c2} and do not follow standard Werthamer-Helfand-Hohenberg theory [14]. However, unlike the pnictides, the Mo_6X_8 (X = S, Se) Chevrel cluster does not exhibit any intrinsic magnetism or competing order. This greatly simplifies the analysis and interpretation of its low-temperature properties, particularly any multiband effects. Band structure calculations have indicated the presence of two Mo d bands at E_F in CPs [15]: In this Letter, we present local spectroscopic evidence for two distinct superconducting gaps in $SnMo_6S_8$ and $PbMo_6S_8$. These data are supported by specific heat measurements displaying clear signatures of a second gap.

We have chosen to focus on $SnMo_6S_8$ and $PbMo_6S_8$ since these two materials have the highest values for T_c and H_{c2} within the CP family: 14.2 K, ~40 T and 14.9 K, >80 T, respectively [16]. Single crystals of each compound with volume ~1 mm^3 were grown at 1600 °C by a chemical flux transport method by using sealed molybdenum crucibles. Their high purity was confirmed by ac susceptibility yielding $\Delta T_c = 0.1$ K for $SnMo_6S_8$ and 0.3 K for $PbMo_6S_8$. Local spectroscopy (STS) was performed on room-temperature-cleaved samples with a home-built helium-3 scanning tunneling microscope in high vacuum ($< 10^{-7}$ mbar), by using a lock-in amplifier technique. Heat capacity measurements were carried out at the Grenoble High Magnetic Field Laboratory by using high-resolution "long relaxation" microcalorimetry [17] and in Geneva with a Quantum Design™ physical property measurement system.

The first hint of a two-band order parameter arises from fast spectroscopic traces over several tens of nanometers in the (001) plane of each material (Fig. 1). The corresponding topography in $SnMo_6S_8$ shows atomically flat terraces separated by steps of size 12 ± 1 Å, which compares favorably with twice the rhombohedral unit-cell parameter 6.5 Å. Spectra taken on the terraces are homogeneous, with a gap of 2.95 meV and a marked lack of any quasiparticle excitations within the gap. In contrast, spectra taken on the steps between terraces consistently display additional kinks at low energy [with fully formed peaks occasionally observed, as in Fig. 1(a)(iv)], which are suggestive of a second gap. We interpret this as a local modification of the

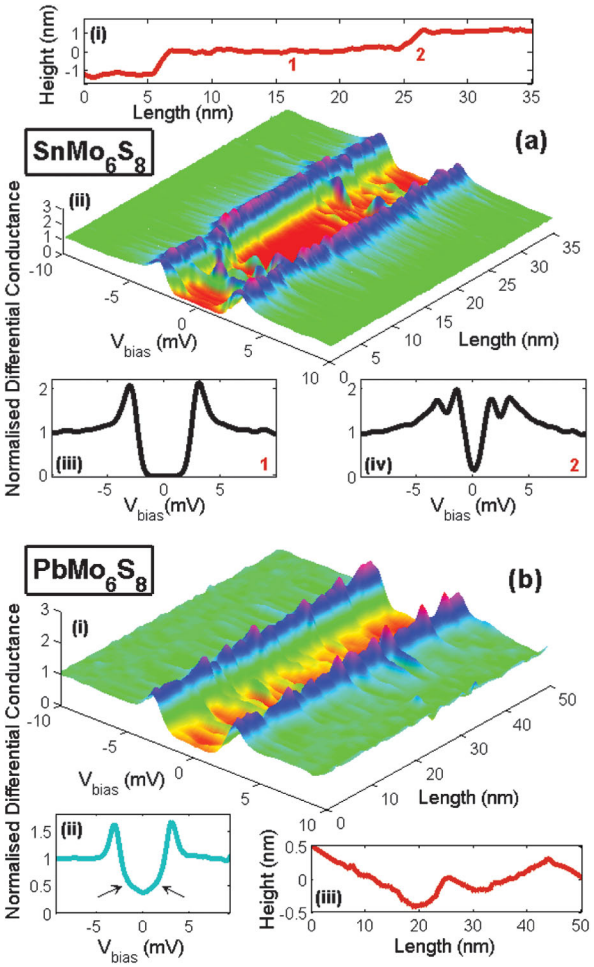

FIG. 1 (color). (a) Zero-field 35 nm trace on $SnMo_6S_8$ taken at $T = 0.4$ K, junction resistance $R_T = 0.03$ GΩ. (i) Topography showing steps two unit cells high; (ii) spectroscopic trace; (iii), (iv) raw spectra taken on a flat terrace (1) and above a topographic step (2). (b) Zero-field 40 nm trace on $PbMo_6S_8$ taken at $T = 0.5$ K, $R_T = 0.015$ GΩ. (i) Spectroscopic trace; (ii) average spectrum from entire trace; (iii) topographic variation.

tunneling matrix element, enabling us to preferentially probe another portion of the Fermi surface with different atomic orbital characters. Cleaved surfaces of $PbMo_6S_8$ are of rather lower quality with an rms roughness of ∼1.5 Å and broad poorly resolved unit-cell-sized steps [Fig. 1(b)(iii)]. However, the average spectrum [Fig. 1(b)(ii)] displays a kink at ∼ ± 1.4 meV (highlighted by arrows) and a V-shaped dispersion around E_F. This confirms the presence of states within the large gap.

Such a dramatic spectral variation as a function of the local topography has not previously been observed in any other superconductor. It may therefore be natural to suggest that the isolated appearance of these multigap signatures at topographic steps could be due to a surface bound state or defect. However, a localized state would not display the particle-hole symmetry of the peaks we observe. We have imaged a large number of separate topographic steps, and a second gap is consistently observed upon scanning across them. Another explanation for the double-gap behavior could be the proximity effect inducing weak superconductivity in a metallic surface layer [18]. However, the small gap induced would vary strongly with the thickness of the surface metallic layer. Apart from the fact that measurements are performed on freshly cleaved samples, thus rendering any surface layer deposition implausible, a layer of metallic impurities would not be expected to have a uniform thickness. This would cause substantial variation in the size of the induced gap and an extremely high zero-bias conductance, both of which are incompatible with our data.

In Fig. 2, we display a range of spectra with fits using a multiband model. The Bardeen-Cooper-Schrieffer (BCS) quasiparticle density of states for an anisotropic s-wave n-band superconductor may be written as

$$N(\omega) = \sum_{j=1}^{n} \frac{N_j}{2\pi} \int_0^{\pi} \mathrm{Re}\left[\frac{(\omega + i\Gamma_j)\mathrm{sgn}(\omega) d\theta}{\sqrt{(\omega + i\Gamma_j)^2 - \Delta_j^2 F_j^2(\theta)}}\right], \quad (1)$$

where N_j is the percentage contribution of band j to the density of states (DOS) at E_F, Γ_j the scattering rate due to lifetime effects, Δ_j the magnitude of the gap within band j, and $F_j(\theta) = a_j + (1 - a_j)\cos\theta$ measures the anisotropy of the corresponding gap with $0.5 < a_j < 1$. We determine the parameters N_j, Δ_j, a_j, and Γ_j by fitting our data to the theoretical DOS convolved with the derivative of the Fermi function at the experimental temperature and a 0.3 meV Gaussian (to account for lock-in smearing). Note that the spectral backgrounds between ±5–10 meV are rather poorly fitted, indicating strong coupling to a low-energy phonon.

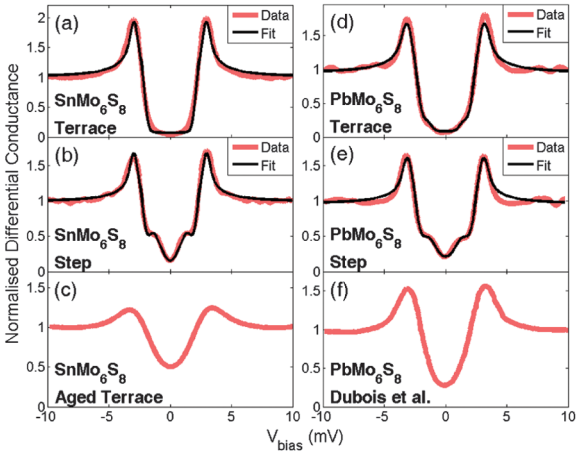

FIG. 2 (color). (a)–(c) $SnMo_6S_8$ spectra and fits: $T = 0.4$ K, $R_T = 0.03$ GΩ. (d)–(e) $PbMo_6S_8$ spectra and fits: $T = 0.5$ K, $R_T = 0.015$ GΩ. (f) $PbMo_6S_8$ spectrum from [19]: $T = 1.9$ K, $R_T = 0.025$ GΩ. See the text for details and Table I for fit parameters. $2\Delta_1/k_BT_c$ in $PbMo_6S_8$ is similar to data from [26].

Atomically flat surfaces in $SnMo_6S_8$ produce homogeneous spectra [Fig. 2(a)] which may be fitted by using a single band [i.e., $n = 1$ in (1)]. There is a slight deterioration in the fit quality at low energy, which is attributed to a very small contribution from band 2. In contrast, Fig. 2(b) shows the average of around 50 spectra acquired above a topographic step. There is clearly a significant contribution from the smaller gap, necessitating a two-band fit. Similar fits are carried out on spectra from a flat zone and a broad step in $PbMo_6S_8$ and the parameters obtained listed in Table I. We find $2\Delta_1/k_BT_c \sim 5$ in each compound, but Δ_2 is 30%–40% larger in $PbMo_6S_8$ than $SnMo_6S_8$. In both materials the gap anisotropies are similar: A small anisotropy in H_{c2} ($\epsilon^2 = 0.67$) has been observed in $PbMo_6S_8$ [3], but with the present data we are unable to judge whether this is due to the anisotropy in Δ_1 or Δ_2. We believe it unwise to draw quantitative conclusions on the symmetry of Δ_2, since our experiment has a finite resolution imposed by a 0.3 meV broadening from the lock-in. However, any interband scattering will preclude a pure d-wave order parameter in Δ_2 due to the dominant isotropic s-wave component in Δ_1.

Previous STS experiments on $PbMo_6S_8$ provided evidence for low-energy excitations within the superconducting gap but lacked sufficient resolution to distinguish two separate gaps. This is due to three factors: sample age, temperature, and environment. In Ref. [19], measurements were performed on old crystals at 1.9 K in an exchange gas, compared with freshly grown samples at 0.4–0.5 K and high vacuum in the present work. The increased thermal broadening at 1.9 K blurs the two gaps, though this should not be sufficient to render the smaller gap invisible. The major factor here is a deterioration in the sample surface due to the exchange gas environment. It is well known that, in a two-band superconductor, interband scattering due to impurities mixes the two gaps and reduces T_c, resulting in an effective single-band anisotropic superconductor in the dirty limit. This was first predicted for MgB_2 [20,21] and later observed in irradiated samples [22]. However, due to extremely weak scattering between σ and π bands, the single-band limit is never reached in MgB_2. This may not be the case for CPs: Figure 2(c) displays a $SnMo_6S_8$ spectrum from a terrace after 3 months of measurements comprising numerous thermal and magnetic cycles. It is qualitatively similar to data from [19] [see Fig. 2(f)], providing good evidence for low-energy states within the large gap, but does not display a distinct smaller gap. This is consistent with the presence of strong interband surface scattering. The zero-bias conductance is also rather high in both (c) and (f), which we attribute to a decrease in the superfluid density due to enhanced pair breaking from inelastic scattering.

Upon increasing the temperature, the large gap is gradually reduced and closes at the bulk T_c determined by ac susceptibility. No pseudogap is visible above T_c, confirming that superconductivity arises from a metallic ground state and hence justifying the use of a BCS model to fit the spectra. In Fig. 3, we have plotted the variation of the large gap Δ_1 with temperature for each compound, with the theoretical BCS weak-coupling s-wave curve for comparison. A small kink is visible within each curve (shaded areas). Similar features have been observed in the temperature variation of the π-band gap in MgB_2 [23] and, strikingly, in the $LaFeAsO_{1-x}F_x$ pnictide [24]. Assuming this kink is a signature of superconductivity in band 2, its position at higher energy in $PbMo_6S_8$ compared to $SnMo_6S_8$ is consistent with our observation that Δ_2 is larger in $PbMo_6S_8$. We hypothesize that this may be the key to $PbMo_6S_8$ having a significantly higher H_{c2} than $SnMo_6S_8$, although further experiments will be required for confirmation.

It is instructive to complement our STS measurements with bulk thermodynamic (HC) data, in order to conclusively rule out any spurious surface effects being responsible for Δ_2. Figures 4(a) and 4(b) display the electronic heat capacity C_{elec} in $SnMo_6S_8$ and $PbMo_6S_8$: This is

TABLE I. Superconducting gap parameters and relative DOS contributions from tunneling (STS) and heat capacity (HC) data. $\Delta_{1,2}$ units are meV; $\Gamma_{1,2} \leq 0.2$ meV for all STS fits.

	$SnMo_6S_8$		$PbMo_6S_8$	
T_c	14.2 ± 0.05 K		14.9 ± 0.15 K	
STS	Terrace	Step	Terrace	Step
Δ_1	2.92 ± 0.1	2.95 ± 0.1	3.14 ± 0.15	3.06 ± 0.15
Δ_2	⋯	1.05 ± 0.2	1.42 ± 0.2	1.36 ± 0.2
a_1	0.85 ± 0.02	0.87 ± 0.02	0.85 ± 0.02	0.89 ± 0.02
a_2	⋯	0.91 ± 0.1	0.92 ± 0.1	0.75 ± 0.1
N_1	⋯	62 ± 4	90 ± 4	66 ± 4
N_2	⋯	38 ± 4	10 ± 4	34 ± 4
HC	Bulk		Bulk	
H_{c2}	42 ± 1 T		86 ± 5 T	
γ	6.4 ± 0.1 mJ gat^{-1} K^{-2}		6.7 ± 0.1 mJ gat^{-1} K^{-2}	
Δ_1	3.06 ± 0.1		3.15 ± 0.1	
Δ_2	0.86 ± 0.1		1.41 ± 0.1	
N_1	96 ± 2		90 ± 2	
N_2	4 ± 2		10 ± 2	

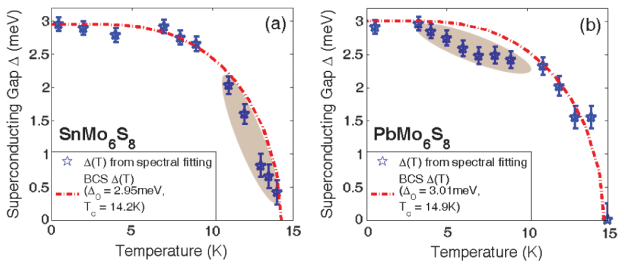

FIG. 3 (color). Temperature variation of the large gap $\Delta_1(T)$ in (a) $SnMo_6S_8$ and (b) $PbMo_6S_8$, measured by STS. The gap value was determined by fitting spectra acquired on a flat terrace (i.e., with a negligible Δ_2 component) using a BCS single-band anisotropic s-wave model.

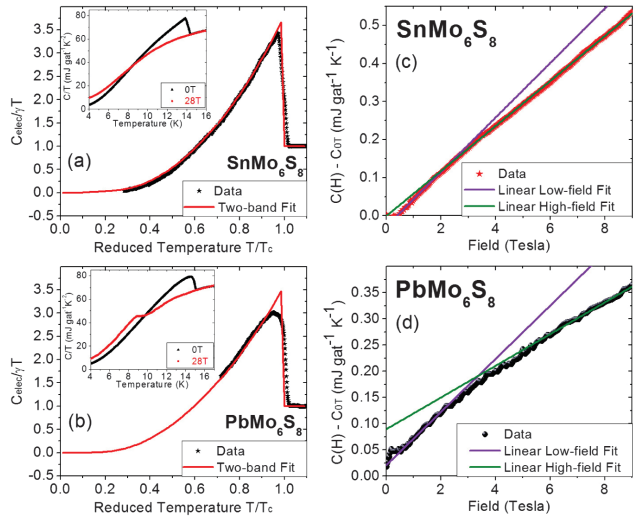

FIG. 4 (color). (a),(b) $C_{\rm elec}/\gamma T$ with two-band α-model fits [25]. Insets: C/T at 0 and 28 T. (c),(d) Field-dependent contributions to $C_{\rm elec}$ at $T = 0.35$ K with linear fits above and below the crossover field H_x (see the text). The crossover in $PbMo_6S_8$ is rather broad compared to $SnMo_6S_8$; this is due to the lower homogeneity in the $PbMo_6S_8$ crystal as seen by increased transition widths in HC and ac susceptibility data.

measured by subtracting the HC in an applied field $H = 28$ T from the zero-field data $C_{0\,\rm T}$. To eliminate the effect of fluctuations above T_c in high field, we limit our data to $T > 1.15T_c(28\ \rm T)$, where $T_c(28\ \rm T) = 4.4$ and 9.3 K in $SnMo_6S_8$ and $PbMo_6S_8$, respectively. In CPs there is a large contribution to the lattice HC $C_{\rm latt}$ from a low-energy Einstein phonon due to vibrations of the cation between the Mo_6X_8 clusters: It is therefore not possible to remove $C_{\rm latt}$ from $C_{0\,\rm T}$ by using the conventional $\Sigma_{j=1}^{n} B_{2j+1}T^{2j+1}$ model. Using a two-band α model [25], we have performed fits to $C_{\rm elec}$ and summarize our results in Table I. Despite the lack of data at low temperature, we may still extract the Sommerfeld constant γ since $\int_0^{T_c}(C_{\rm elec} - \gamma T)/T\ dT$ must equal zero (to conserve entropy). We find that $\gamma/T_c = 0.45\ \rm mJ\,gat^{-1}\,K^{-3}$ in each compound, suggesting that T_c scales with the DOS at E_F. For both gaps, the ratios $2\Delta_j/k_BT_c$ from our STS data agree perfectly with those from HC experiments. While it is not possible to quantitatively compare our STS-measured N_j (which also depends on the tunneling matrix element) with the bulk N_j, the trends observed by each technique ($N_1 > N_2$) are qualitatively in agreement.

The final signature of two-band superconductivity is provided by the low-temperature variation of $C_{\rm elec}(H)$ in each material. In a single-band BCS s-wave superconductor, $\gamma(H)$ should be linear. However, at $T = 0.35$ K we observe bends in $C_{\rm elec}(H)$ at $H_x = 2.8 \pm 0.2$ and 3.4 ± 1 T in $SnMo_6S_8$ and $PbMo_6S_8$, respectively, reminiscent of the low-field behavior of MgB_2 [22]. Extrapolating the high-field linear fits to the normal-state γ value yields $H_{c2} = 42 \pm 1$ and 86 ± 5 T (although these may be slight overestimates due to vortex overlap effects at high field). We assume that H_x corresponds to the crossover between filling Δ_2 in band 2 followed by Δ_1 in band 1, i.e., $H_x/H_{c2} = N_2/(N_1 + N_2)$ and hence $N_1 = 93 \pm 0.5$, $N_2 = 7 \pm 0.5$ and $N_1 = 96 \pm 1$, $N_2 = 4 \pm 1$ for $SnMo_6S_8$ and $PbMo_6S_8$. These figures are in good agreement with those in Table I.

Together, our spectroscopic and thermodynamic data provide compelling evidence for a multiband order parameter in CP superconductors. In both $SnMo_6S_8$ and $PbMo_6S_8$, a strongly coupled quasi-isotropic band (contributing the majority of the DOS at E_F) coexists with a highly anisotropic weakly coupled minority band. Looking ahead, we postulate that understanding and manipulating the interplay between two or more such bands may hold the secret to realizing high values for H_{c2} in future superconducting materials.

[1] Ø. Fischer, Appl. Phys. **16**, 1 (1978).
[2] R. Chevrel, M. Sergent, and J. Prigent, J. Solid State Chem. **3**, 515 (1971).
[3] M. Decroux and Ø. Fischer, *Topics in Current Physics: Superconductivity in Ternary Compounds II* (Springer-Verlag, Berlin, 1982), pp. 57–87.
[4] H. Suhl, B. Matthias, and L. Walker, Phys. Rev. Lett. **3**, 552 (1959).
[5] L. Shen, N. Senozan, and N. Phillips, Phys. Rev. Lett. **14**, 1025 (1965).
[6] G. Binnig *et al.*, Phys. Rev. Lett. **45**, 1352 (1980).
[7] J. Nagamatsu *et al.*, Nature (London) **410**, 63 (2001).
[8] M. R. Eskildsen *et al.*, Phys. Rev. B **68**, 100508 (2003).
[9] F. Bouquet *et al.*, Phys. Rev. Lett. **89**, 257001 (2002).
[10] B. Bergk *et al.*, Phys. Rev. Lett. **100**, 257004 (2008).
[11] S. Kuroiwa *et al.*, Phys. Rev. Lett. **100**, 097002 (2008).
[12] R. Hill *et al.*, Phys. Rev. Lett. **101**, 237005 (2008).
[13] F. Hunte *et al.*, Nature (London) **453**, 903 (2008).
[14] N. Werthamer, E. Helfand, and P. Hohenberg, Phys. Rev. **147**, 295 (1966).
[15] O. K. Andersen, W. Klose, and H. Nohl, Phys. Rev. B **17**, 1209 (1978).
[16] Previous experiments on $PbMo_6S_8$ in the 1970s suggested $H_{c2} \sim 55$–60 T. However, recent data from oxygen-free crystals (including our specific heat-derived value in Table I) reveal a significantly higher H_{c2} of at least 80 T.
[17] R. Lortz *et al.*, Phys. Rev. Lett. **99**, 187002 (2007).
[18] W. L. McMillan, Phys. Rev. **175**, 537 (1968).
[19] C. Dubois *et al.*, Phys. Rev. B **75**, 104501 (2007).
[20] A. Y. Liu, I. Mazin, and J. Kortus, Phys. Rev. Lett. **87**, 087005 (2001).
[21] I. Mazin *et al.*, Phys. Rev. Lett. **89**, 107002 (2002).
[22] Y. Wang *et al.*, J. Phys. Condens. Matter **15**, 883 (2003).
[23] F. Bobba *et al.*, Supercond. Sci. Technol. **16**, 167 (2003).
[24] R. Gonnelli *et al.*, Phys. Rev. B **79**, 184526 (2009).
[25] H. Padamsee, J. Neighbor, and C. Shiffman, J. Low Temp. Phys. **12**, 387 (1973).
[26] U. Poppe and H. Wühl, J. Low Temp. Phys. **43**, 371 (1981).